Letter

Clean-limit superconductivity in $Im\bar{3}m$ H_3S synthesized from sulfur and hydrogen donor ammonia borane

Israel Osmond,[1] Owen Moulding,[1] Sam Cross,[1] Takaki Muramatsu,[1] Annabelle Brooks,[1] Oliver Lord,[2] Timofey Fedotenko,[3] Jonathan Buhot,[1] and Sven Friedemann[1,*]

[1]*H.H. Wills Physics Laboratory, University of Bristol, Bristol BS8 1TL, United Kingdom*

[2]*School of Earth Sciences, University of Bristol, Wills Memorial Building, Queen's Road, Bristol BS8 1RJ, United Kingdom*

[3]*Photon Science, DESY, 22607 Hamburg, Germany*

(Received 21 March 2022; revised 6 May 2022; accepted 13 May 2022; published 6 June 2022)

We present detailed studies of the superconductivity in high-pressure H_3S. X-ray diffraction measurements show that cubic $Im\bar{3}m$ H_3S was synthesized from elemental sulfur and hydrogen donor ammonia borane (NH_3BH_3). Our electrical transport measurements confirm superconductivity with a transition temperature $T_c = 197$ K at 153 GPa. From the analysis of both the normal-state resistivity and the slope of the critical field, we conclude that the superconductivity is described by clean-limit behavior. A significant broadening of the resistive transition in finite magnetic field is found, as expected for superconductors. We identify a linear temperature-over-field scaling of the resistance at the superconducting transition which is not described by existing theories.

DOI: 10.1103/PhysRevB.105.L220502

The discovery of superconductivity in H_3S at a critical temperature of $T_c \sim 200$ K revolutionized the search for high-temperature superconductivity [1]. Since then, high-temperature superconductivity has been observed in a number of binary hydrides at high pressures including LaH_{10}, CeH_9, and YH_9 and in carbonaceous sulfur hydride [1–6]. Extreme pressures of typically more than 100 GPa are required for the synthesis and study of these hydride compounds. The high hydrogen stoichiometries yield the high density of electronic states, high-frequency phonon modes, and strong electron-phonon coupling necessary for a high-T_c in phonon-mediated superconductivity [5–9]. Both synthesis and experimental studies of high-temperature hydride superconductors remain very challenging due to the high pressures needed.

Synthesis of hydride superconductors is typically done by laser heating precursors *in situ* at high pressures. Only in the initial work by Drozdov *et al.* was superconducting H_3S synthesized from the dissociation of molecular H_2S at high pressures [1,10–12]. All recent studies synthesized H_3S from elemental sulfur and either molecular hydrogen or a hydrogen donor material as precursors using laser heating [3,13–19]. While molecular hydrogen affords the cleanest synthesis route, loading hydrogen into a diamond anvil cell (DAC) is technically much more demanding. Thus, it is not easily adapted for widespread and detailed studies of superconductivity in hydrides by the global physics community. Hence, it is important to establish synthesis routes using hydrogen donor materials like ammonia borane. For some hydrides this can be further simplified with evaporated samples of starting elements such as yttrium or lanthanum [17,20].

Detailed understanding of the superconductivity in hydride compounds requires structural information, e.g., from x-ray diffraction (XRD) to complement information about the superconducting properties—ideally on the same sample. Transition temperatures up to 203 K have been linked to the cubic $Im\bar{3}m$ phase of H_3S at a pressure of 155 GPa [1,21]. At pressures below ≈140 GPa a rhombohedral distortion leads to a lower symmetry $R3m$ phase with a reduced T_c [22]. Other phases have been reported but have not been probed for superconductivity [10,11,14,15,19].

Superconductivity in H_3S has been confirmed with multiple probes despite the limitations and challenges of measurements in DACs. The most common evidence stems from the observation of zero resistance for various samples by the group of Eremets and the suppression of the resistive transition in magnetic field [1,13,21]. In addition, a suppression of T_c has been observed for samples with deuterium substitution [1,21], roughly in agreement with the expected isotope effect predicted by computational studies [7,23]. A diamagnetic signal has been observed in dc magnetization measurements [1,18], nuclear resonant scattering [24], and in ac susceptibility in Ref. [12]. Recently, Minkov *et al.* have presented detailed magnetization studies of H_3S synthesized from sulfur and ammonia borane from which they extract the lower critical field and London penetration depth [18]. Here we present electrical resistance measurements demonstrating superconductivity in H_3S synthesized with this novel route using ammonia borane and sulfur.

Our successful synthesis of $Im\bar{3}m$ H_3S is evident from the XRD data collected on our sample at 153 GPa as presented in Fig. 1. After loading sulfur and ammonia borane, we applied 153 GPa and subsequently laser heated the sample in a small area (cf. Sec. I of the Supplemental Material for synthesis details [25,26]). In the laser-heated area, we clearly observe

*Sven.Friedemann@bristol.ac.uk

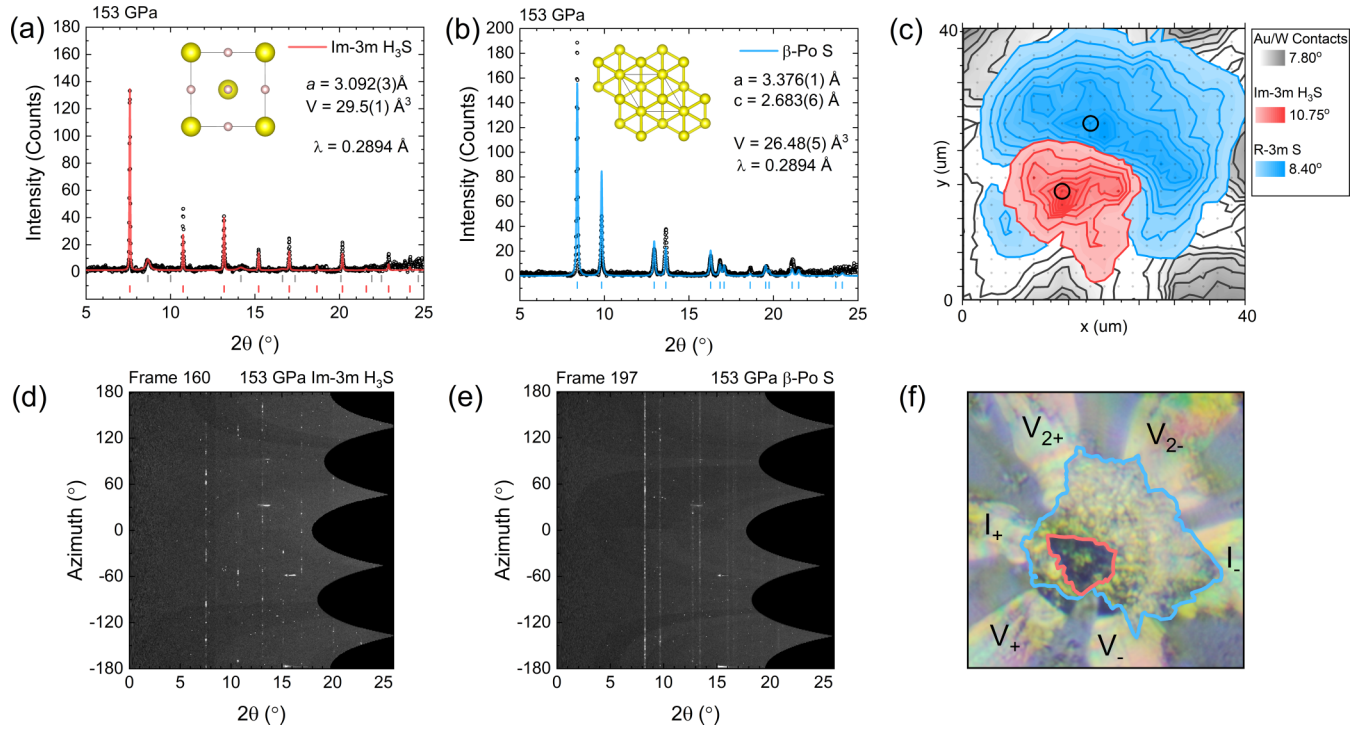

FIG. 1. Powder x-ray diffraction showing $Im\bar{3}m$ H_3S. Powder patters taken with a 30-s acquisition time and corrected for diffuse scattering. Panels (a) and (b) show the integrated patterns at locations where $Im\bar{3}m$ H_3S and elemental sulfur (S-V) are respectively present. Vertical ticks indicate expected peak positions for the different phases (gray corresponds to cubic boron nitride). (c) Spatial mapping of Bragg reflections associated with S-V and $Im\bar{3}m$ H_3S phases. Contacts visible in gray, with the S-V and H_3S regions shown in blue and red, respectively. [(d) and (e)] Unfurled area detector images of powder patterns presented in (a) and (b). Diffuse background correction details are discussed in Sec. SII of the Supplemental Material [25]. (f) Photo of the sample. Labels mark the electrical contacts, while the blue and red lines demarcate the sulfur and H_3S respectively.

an XRD pattern in excellent agreement with $Im\bar{3}m$ H_3S as demonstrated in Fig. 1(a) (see Sec. II of the Supplemental Material [25] and references therein [27,28] for details of the XRD measurements). In particular, we observe no splitting of the (110) Bragg peak at $2\theta = 7.6^\circ$ and hence conclude that a rhombohedral distortion is absent in our sample. This is in agreement with the stability range of the $Im\bar{3}m$ phase above 140 GPa established from previous XRD measurements [10]. The $Im\bar{3}m$ phase in our sample consists of larger crystallites compared to the elemental sulfur as evident from the spots in the detector images Figs. 1(d) and 1(e). Yet a preferred orientation appears to be absent as indicated by the good agreement with the Rietveld refinement of the XRD pattern in Fig. 1(a). For the $Im\bar{3}m$ H_3S phase, we find a unit cell volume of 29.5(1) $Å^3$, in good agreement with previous calculations (29.2 $Å^3$) [29] and with earlier XRD studies at similar pressures (29.8 $Å^3$) where H_3S is synthesized using elemental precursors [10,22]. Outside the laser-heated area, we find XRD patterns in excellent agreement with elemental sulfur (S-V) in its rhombohedral β-Po structure [cf. Fig. 1(b)].

Both the XRD mapping and optical image [Figs. 1(c) and 1(f)] of our sample demonstrate that $Im\bar{3}m$ H_3S has formed in an area of $\approx 15 \times 15$ μm. In the optical image, this region is darker than the grainy, metallic elemental sulfur surrounding it and contains a reflective region in its center. This black region likely marks boron nitride residue from the dissociation of ammonia borane, with weak Bragg reflections associated with boron nitride also visible in Fig. 1(a), while the central reflective area constitutes an exposed surface of $Im\bar{3}m$ H_3S with metallic reflectivity. Below, we demonstrate that $Im\bar{3}m$ H_3S in our sample displays metallic electrical resistance. The XRD mapping of the characteristic peaks (Fig. 1) confirms that the entire dark region (including the reflective center) has been transformed to $Im\bar{3}m$ H_3S while the remainder of the sample is pure elemental sulfur. In addition, we observe the XRD peaks of tungsten and gold from our electrodes at the outer edges of the area scanned with XRD [gray areas in Fig. 1(c)].

Formation of superconducting $Im\bar{3}m$ H_3S in our sample is evident from resistivity measurements presented in Fig. 2, which show a large drop in resistance ($\approx$80%) at $T_c = 197$ K (see SI III for further details). Before laser heating, we observe the expected behavior of elemental sulfur at high pressure: The resistance is metallic and features the superconducting transition of elemental sulfur at 17 K [30,31]. After laser heating, the resistance shows a major drop at $T_c = 197$ K which we associate with the formation of superconducting H_3S. Below T_c, a residual resistance of $\approx$20% remains which stems from residual elemental sulfur in the measurement path using the contacts $V\pm$. With six electrodes, the voltage drop associated with the superconducting transition can be measured in four-point configuration on both sides of the sample. Using the electrodes [labelled $V\pm$ in Fig. 1(f)] close to the $Im\bar{3}m$ H_3S part of the sample we find an 80% drop of the resistance.

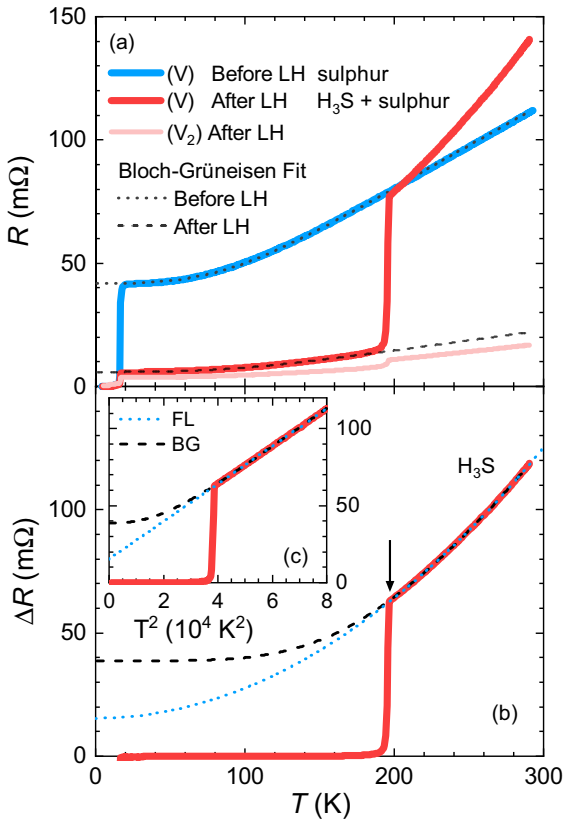

FIG. 2. High T_c superconducting H_3S. (a) Electrical resistance before and after laser heating (LH) measured on two different pairs of contacts [cf. labels in Fig. 1(f)]. The normal resistance of elemental sulfur before laser heating (blue) has been fitted with Eq. (1) (dotted line) for $20\,\mathrm{K} \leqslant T \leqslant 290\,\mathrm{K}$. The contribution from sulfur after laser heating has been fitted for $35\,\mathrm{K} \leqslant T \leqslant 150\,\mathrm{K}$ with Eq. (1) (dashed line) using Θ_D and n found for elemental sulfur before laser heating. (b) The contribution from H_3S has been extracted by subtracting the Bloch-Grüneisen (BG) form of the residual sulfur [dashed line in (a)]. Vertical arrow marks $T_c = 197\,\mathrm{K}$ taken as the intersection between linear fits to the superconducting transition and to the normal-state resistance. Bloch-Grüneisen and Fermi-liquid (FL) fits to the normal-state resistance of H_3S ($T \leqslant 205\,\mathrm{K}$) are shown as dashed and dotted lines, respectively. Inset (c) shows the resistance of H_3S versus T^2 together with both fits.

By contrast, the electrodes further away (labelled $V_2\pm$) yield a drop of less than 25 %. This shows that superconducting H_3S is present closer to the electrodes $V\pm$ while unreacted sulfur dominates the transport behavior sensed between electrodes $V_2\pm$. Hence, we associate the resistive transition with superconductivity of the $Im\bar{3}m$ phase detected close to the $V\pm$ electrodes.

The resistance contribution originating from H_3S is extracted in Fig. 2(b). Here the residual resistance from elemental sulfur is subtracted over the full temperature range. For this, we identify the parameters describing the normal-state resistance of elemental sulfur from a Bloch-Grüneisen (BG) fit

$$R(T) = R_0 + B\left(\frac{T}{\Theta_D}\right)^n \int_0^{\Theta_D/T} \frac{z^n dz}{(e^z - 1)(1 - e^{-z})} \quad (1)$$

between $20\,\mathrm{K} \leqslant T \leqslant 150\,\mathrm{K}$ as shown by the dotted line in Fig. 2(a). Here R_0 is the residual resistance of the normal state, B quantifies the magnitude of the resistance contribution from electron-phonon scattering, and Θ_D is the Debye temperature. The exponent n assumes different values depending on whether scattering is intraband ($n = 5$) or interband ($n = 3$) [32]. We use parameters specific to elemental sulfur established from fits to $R(T)$ before laser heating as shown by the dotted line in Fig. 2: $\Theta_D = 680\,\mathrm{K}$ and $n = 3$. These parameters are in good agreement with recent calculations for elemental sulfur which predicts strong interband scattering [33]. With Θ_D and n fixed, only R_0 and B are fitted to the sulfur contribution in the resistance after laser heating [dashed line in Fig. 2(a)] [34]. We find that the ratio B/R_0 is increased by ≈40 % for the sulfur contribution after laser heating compared to before laser heating. This suggests that the laser heating has annealed the elemental sulfur and reduced the concentration of dislocations and/or grain boundaries. We obtain the resistance contribution (ΔR) of H_3S by subtracting the fit representing the residual sulfur. This corresponds to the assumption of a series-resistor network which is guaranteed below T_c by the superconducting state of H_3S and likely satisfied above T_c given the proximity of the sensing electrodes to the H_3S phase in our sample. The resulting curve for the resistance of H_3S is shown in Fig. 2(b).

The normal state behavior of $Im\bar{3}m$ H_3S can be well fitted by the BG form [Eq. (1)] as shown by the dashed line in Fig. 2(b). The limited temperature range of the normal state ($200\,\mathrm{K} \leqslant T \leqslant 300\,\mathrm{K}$) does not allow us to determine the exponent n for H_3S, and $n = 3$ and $n = 5$ yield very similar fits to the data. We fix the exponent to the most common value $n = 5$, i.e., assuming that intraband scattering is dominant in $Im\bar{3}m$ H_3S, but highlight the resulting uncertainty to other quantities. We find a Debye temperature $\Theta_D = 1260\,\mathrm{K}$ ($\Theta_D = 1570\,\mathrm{K}$ for $n = 3$) that is considerably larger than for elemental sulfur, reflecting the increased phonon energies stemming from lattice vibrations involving hydrogen. Θ_D is in good agreement with the characteristic phonon frequency calculated by Errea *et al.* [7]. We note that the Fermi-liquid (FL) quadratic temperature dependence of the resistance ($R = R_0 + AT^2$) discussed in previous work [13] is consistent with the crossover range of the BG form as shown in the inset Fig. 2(c). However, the magnitude of the temperature-dependent resistance is much more consistent with the electron-phonon scattering associated with the BG form than the electron-electron scattering associated with the FL form. Specifically, using the lateral dimensions $15 \times 15\,\mu\mathrm{m}$ and a plausible thickness of 2 μm of the H_3S phase of the sample, we estimate the resistivity and the specific magnitude $B' = 7 \times 10^{-9}\,\Omega\mathrm{m}$ of the electron-phonon contribution as well as the specific magnitude of the FL contribution $A' = 2.4 \times 10^{-12}\,\Omega\mathrm{m\,K^{-12}}$. While the uncertainty of A' and B' is dominated by the uncertainty of the sample thickness ≈50% we can compare to values for other metals. B' is comparable in magnitude to values for simple monovalent metals [32] but A' is at least one order of magnitude larger than for transition metals [35]. Hence, this comparison suggests that the normal-state resistance of $Im\bar{3}m$ H_3S is dominated by electron-phonon scattering.

We estimate the mean free path in our H_3S sample to be $l \approx 8\,\mathrm{nm}$. For this, we use the sample dimensions of the H_3S

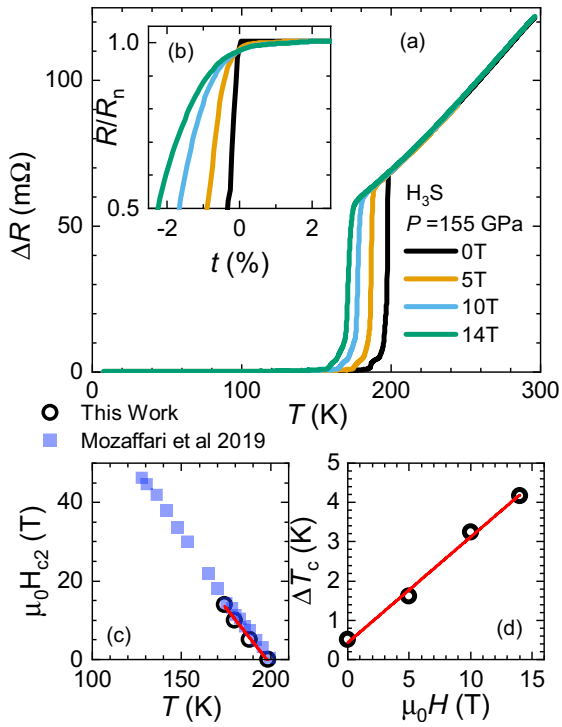

FIG. 3. Suppression of superconducting transition in magnetic field. Resistance versus temperature in magnetic fields. Residual resistance has been subtracted following the procedure outlined in Fig. 2. Inset (b) shows the resistance normalized to normal state versus reduced temperature $t = (T - T_c)/T_c$. Panel (c) shows the upper critical field versus the critical temperature. Here $H_{c2}(T)$ was obtained following $T_c(H)$ taken as the onset of superconductivity determined as the intersection between the normal state behavior and a linear fit to the transition. Previous $H_{c2}(T)$ data at 155 GPa taken from Mozaffari *et al.* [13] are included for comparison. Panel (d) shows ΔT_c, the width of the superconducting transition as a function of magnetic field, given as the difference between T_c onset and the temperature at 50 % of the normalized drop in resistance.

part to estimate the residual resistivity $\rho_0 \approx 8 \times 10^{-8}\,\Omega$m and the Drude transport equation applied to a single-band free-electron approximation $l = \hbar(3\pi^2)^{1/3}/(n^{2/3}e^2\rho_0)$ with the charge carrier concentration $n \approx 8.5 \times 10^{22}\,/\,\mathrm{cm}^3$ determined from Hall effect measurements [13].

Further evidence for the superconducting nature of the transition at $T_c = 197$ K stems from our measurements in magnetic fields up to 14 T. In Fig. 3(a), we show that the transition is shifted to lower temperature in magnetic field. The temperature dependence of the upper critical field, $H_{c2}(T)$, associated with superconductivity of H_3S is in agreement with the behavior reported earlier by Mozaffari *et al.* [cf. Fig. 3(c)] [13]. Our samples and those of Mozaffari *et al.* have been synthesized with different methods, from sulfur and ammonia borane or hydrogen, respectively. This is very likely to lead to different concentrations of impurities as indicated by the difference of resistance ratios at room temperature and low temperature estimated for the normal-state $RRR = R(300\,\mathrm{K})/R_{\mathrm{normal}}(T \to 0) = 3$ and $r = 1.9$ for our sample and that of Mozaffari *et al.*, respectively. The fact that we observe good agreement of $B_{c2}(T)$ between our samples and those of Mozaffari *et al.* suggests that the superconducting properties are independent of impurity concentrations, i.e., in the clean limit. By contrast, the samples obtained via dissociation of H_2S by Drozdov *et al.* [1] showed a much smaller resistance ratio $r \sim 1$ and a larger slope at the critical field, suggesting an enhancement due to a limited mean free path, i.e., in the dirty limit.

The upper critical field of a superconductor is determined by the orbital and Pauli pair-breaking effects. Near T_c, the Pauli pair breaking is negligible for conventional superconductors and, hence, we use the slope of the critical field $dB_{c2}/dT = -0.58(3)\,\mathrm{T\,K}^{-1}$ to estimate the coherence length, ξ_0, and Fermi velocity, v_F. In the clean limit, the slope of the critical field is given by

$$-\left.\frac{dB_{c2}}{dT}\right|_{T_c} = \frac{\Phi_0}{2\pi(0.74)^2\xi_0^2 T_c}, \tag{2}$$

where $\Phi_0 = h/2e$ is the flux quantum. From this, we obtain the coherence length $\xi_0 = 2.2$ nm. Comparison of the coherence length with the mean free path ($\xi_0 < l$) justifies applicability of the clean limit relations. We estimate the Fermi velocity using

$$\xi_0 = \frac{\hbar v_F}{\pi\Delta_0} \approx \frac{\hbar v_F}{\pi\gamma k_B T_c}, \tag{3}$$

where the numerical factor $\gamma \approx 2.0(4)$ reflects the expected strong-coupling behavior associated with the high-temperature superconductivity in H_3S. Based on these assumptions, we obtain $v_F^{\mathrm{exp}} = 3.8(7) \times 10^5\,\mathrm{ms}^{-1}$.

The obtained Fermi velocity is significantly lower than expected from Density Functional Theory (DFT) calculations. We employ Wien2k to calculate the band structure of H_3S based on the experimental lattice parameters from our XRD results. (Details of the DFT calculation can be found in Sec. IV of the Supplemental Material [25] and references therein [36,37].) Our band structure looks very similar to earlier reports [38]. The Fermi velocity at the Fermi energy is shown as a colormap plot over the Fermi surface in Fig. 4. A considerable variation of v_F is found over several of the Fermi-surface sheets. Within a simple single-band model we can compare the global average of the Fermi velocity $\langle v_F^{\mathrm{DFT}}\rangle = 1.6 \times 10^6\,\mathrm{ms}^{-1}$ with our experimental result $v_F^{\mathrm{exp}} \approx 3.8 \times 10^5\,\mathrm{ms}^{-1}$. The reduced Fermi velocity in experiment compared to DFT confirms strong renormalization of the Fermi velocity due to the strong electron-phonon coupling in H_3S [8].

We observe a clear broadening of the superconducting transition in magnetic field. The width of the superconducting transition can be influenced by many factors including inhomogeneities in composition and pressure. In zero field, our sample features a sharp transition with $\Delta T_c = T_c^{\mathrm{onset}} - T_c^{50\,\%} = 0.5$ K, suggesting a good homogeneity of our sample and small pressure gradients. On application of a magnetic field, $\Delta T_c(H)$ increases linearly as demonstrated in Fig. 3(d). A similar linear form with offset has been reported for YH_9 [17]. The broadening of the transition is most visible in the inset Fig. 2(b). An increase in transition width is in general agreement with expectations for a superconducting state [39].

In finite magnetic field, flow of the flux lattice can increase the width of the superconducting transition. Near T_c,

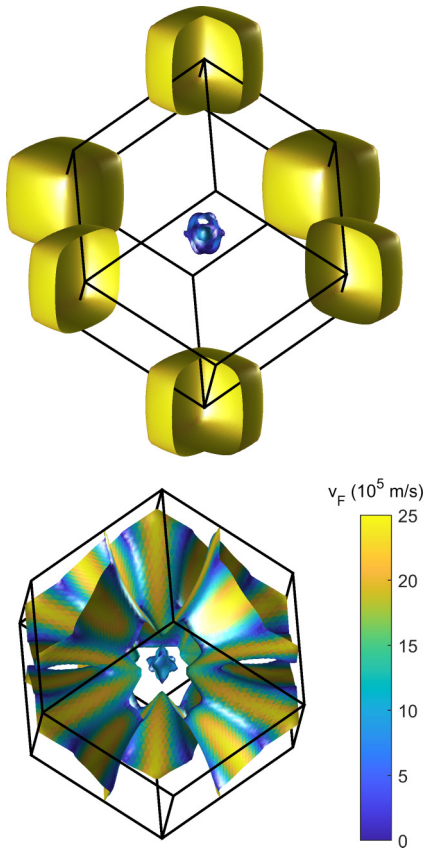

FIG. 4. The magnitude of the Fermi velocity is shown as color map over the Fermi surface of H_3S as obtained with DFT calculations. Fermi surface sheets 1, 3, and 5 are shown in the top panel and sheets 2 and 4 in the bottom panel.

the flow of the flux lattice is determined by the activation energy required to overcome pinning leading to the expectation that the resistance scales as $t^{3/2}/h$ [40]. Here $t = (T - T_c)/T_c$ is the normalized temperature and $h = B/B_{c2}(T = 0)$ the normalized field. Alternatively, the suppression of filamentary superconductivity in finite magnetic fields can cause changes to the superconducting transition—usually leading to a sharper transition with a lower T_c. By analyzing the scaling behavior of a large portion of the resistive transition, we focus on the contributions arising from the bulk of our H_3S phase—the suppression of filamentary superconductivity does not usually lead to a scaling form of the resistance. In our sample of H_3S, we find reasonable scaling of a large proportion of the superconducting transition as demonstrated in Fig. 5. Good scaling is found for a functional form,

$$\frac{R}{R_{\text{normal}}} = f\left(\frac{t^{\beta}}{h+\alpha}\right), \tag{4}$$

linear in temperature, i.e., with $\beta = 1$. To determine h, we use $B_{c2}(T = 0) = 88\,\text{T}$ estimated by Mozaffari *et al.* [13]. The constant $\alpha = 0.019$ reflects the finite width of the superconducting transition in zero magnetic field associated with small sample inhomogeneities, strain, or other nonthermal causes, suggesting that Eq. (4) implies a temperature-over-field scaling of the intrinsic superconducting transition in H_3S. Notably, the scaling of Eq. (4) leads to much better

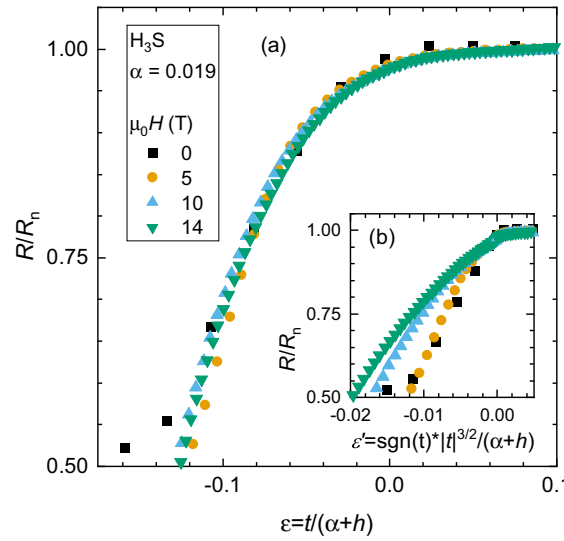

FIG. 5. Scaling analysis of the superconducting transition in finite magnetic fields. The resistance normalized to the normal-state resistance determined from Bloch-Grüneisen fits to the data well above T_c. In (a) R/R_n is shown against $\epsilon = t/(h+\alpha)$ where $t = (T - T_c)/T_c$ is the normalized temperature and $h = B/B_{c2}(T = 0)$ the normalized field. We use $B_{c2} = 88\,\text{T}$ as determined by Ref. [13]. In (b) the normalized resistance is shown against $\epsilon' = \text{sgn}(t)|t|^{3/2}/(h+\alpha)$.

collapse of the data than a form involving $\beta = 3/2$ predicted by Tinkham *et al.* [40] [cf. Fig. 5(b)]. While a precise determination of β, i.e., discriminating exponents close to unity will require further measurements over a wider field range the quality of the data collapse in Fig. 5 suggests that linear temperature-over-field scaling dominates the fluctuations of the superconducting transition in H_3S. A linear form Eq. (4) is consistent with data on MgB_2 and other hydride superconductors [41]. Yet we note that the linear transition width and linear temperature-over-field scaling in H_3S cannot be associated with granular anisotropic superconductivity like in MgB_2 [42] as H_3S is cubic. Hence, the linear temperature-over-field scaling of the resistance in H_3S suggest that a new model might be required to describe the broadening of the superconducting transition in hydride superconductors.

$Im\bar{3}m$ H_3S can be synthesized from elemental sulfur and ammonia borane. Superconductivity is evident from a sudden drop in resistance which is found to shift to lower temperatures and broaden on application of magnetic field. Two experimental observations suggest that the superconductivity follows clean-limit behavior. (i) The critical field curve is found to be identical for different samples at the same pressure synthesised in different ways, i.e., independent of different levels of impurities. (ii) Our estimated mean free path is longer than the coherence length extracted from the slope of the critical field. A significant broadening of the superconducting transition in finite field is found and follows a linear $t/(h+\alpha)$ scaling which suggests that a new model is required to describe the fluctuations in proximity to the superconducting transition in hydrides.

Data are available at the University of Bristol data repository [43].

The authors thank Antony Carrington for valuable discussions. This work was partially supported by the EPSRC under Grants No. EP/V048759/1 and No. EP/L015544/1, as well as the ERC Horizon 2020 programme under Grant No. 715262-HPSuper. O.L. acknowledges support from the Royal Society in the form of a University Research Fellowship (UF150057). We acknowledge DESY (Hamburg, Germany), a member of the Helmholtz Association HGF, for the provision of experimental facilities. Parts of this research were carried out at PETRA III and we thank Hanns-Peter Liermann for assistance in using P02.2. Beamtime was allocated for Proposal No. I-20210376 EC.

[1] A. P. Drozdov, M. I. Eremets, I. A. Troyan, V. Ksenofontov, and S. I. Shylin, Nature (London) **525**, 73 (2015).

[2] W. Chen, D. V. Semenok, X. Huang, H. Shu, X. Li, D. Duan, T. Cui, and A. R. Oganov, Phys. Rev. Lett. **127**, 117001 (2021).

[3] E. Snider, N. Dasenbrock-Gammon, R. McBride, M. Debessai, H. Vindana, K. Vencatasamy, K. V. Lawler, A. Salamat, and R. P. Dias, Nature (London) **586**, 373 (2020).

[4] M. Somayazulu, M. Ahart, A. K. Mishra, Z. M. Geballe, M. Baldini, Y. Meng, V. V. Struzhkin, and R. J. Hemley, Phys. Rev. Lett. **122**, 027001 (2019).

[5] P. Kong, V. S. Minkov, M. A. Kuzovnikov, A. P. Drozdov, S. P. Besedin, S. Mozaffari, L. Balicas, F. F. Balakirev, V. B. Prakapenka, S. Chariton, D. A. Knyazev, E. Greenberg, and M. I. Eremets, Nat. Commun. **12**, 5075 (2021).

[6] A. P. Drozdov, P. P. Kong, V. S. Minkov, S. P. Besedin, M. A. Kuzovnikov, S. Mozaffari, L. Balicas, F. F. Balakirev, D. E. Graf, V. B. Prakapenka, E. Greenberg, D. A. Knyazev, M. Tkacz, and M. I. Eremets, Nature (London) **569**, 528 (2019).

[7] I. Errea, M. Calandra, C. J. Pickard, J. R. Nelson, R. J. Needs, Y. Li, H. Liu, Y. Zhang, Y. Ma, and F. Mauri, Nature (London) **532**, 81 (2016).

[8] I. Errea, F. Belli, L. Monacelli, A. Sanna, T. Koretsune, T. Tadano, R. Bianco, M. Calandra, R. Arita, F. Mauri, and J. A. Flores-Livas, Nature (London) **578**, 66 (2020).

[9] C. J. Pickard, I. Errea, and M. I. Eremets, Annu. Rev. Condens. Matter Phys. **11**, 57 (2020).

[10] A. F. Goncharov, S. S. Lobanov, I. Kruglov, X.-M. Zhao, X.-J. Chen, A. R. Oganov, Z. Konôpková, and V. B. Prakapenka, Phys. Rev. B **93**, 174105 (2016).

[11] Y. Li, L. Wang, H. Liu, Y. Zhang, J. Hao, C. J. Pickard, J. R. Nelson, R. J. Needs, W. Li, Y. Huang, I. Errea, M. Calandra, F. Mauri, and Y. Ma, Phys. Rev. B **93**, 020103(R) (2016).

[12] X. Huang, X. Wang, D. Duan, B. Sundqvist, X. Li, Y. Huang, H. Yu, F. Li, Q. Zhou, B. Liu, and T. Cui, Natl. Sci. Rev. **6**, 713 (2019).

[13] S. Mozaffari, D. Sun, V. S. Minkov, A. P. Drozdov, D. Knyazev, J. B. Betts, M. Einaga, K. Shimizu, M. I. Eremets, L. Balicas, and F. F. Balakirev, Nat. Commun. **10**, 2522 (2019).

[14] E. J. Pace, S. E. Finnegan, C. V. Storm, M. Stevenson, M. I. McMahon, S. G. MacLeod, E. Plekhanov, N. Bonini, and C. Weber, Phys. Rev. B **102**, 094104 (2020).

[15] B. Guigue, A. Marizy, and P. Loubeyre, Phys. Rev. B **95**, 020104(R) (2017).

[16] H. Nakao, M. Einaga, M. Sakata, M. Kitagaki, K. Shimizu, S. Kawaguchi, N. Hirao, and Y. Ohishi, J. Phys. Soc. Jpn. **88**, 123701 (2019).

[17] E. Snider, N. Dasenbrock-Gammon, R. McBride, X. Wang, N. Meyers, K. V. Lawler, E. Zurek, A. Salamat, and R. P. Dias, Phys. Rev. Lett. **126**, 117003 (2021).

[18] V. Minkov, S. Bud'ko, F. Balakirev, V. Prakapenka, S. Chariton, R. Husband, H.-P. Liermann, and M. Eremets, Nature Portfolio (2021), doi: 10.21203/rs.3.rs-936317/v1.

[19] D. Laniel, B. Winkler, E. Bykova, T. Fedotenko, S. Chariton, V. Milman, M. Bykov, V. Prakapenka, L. Dubrovinsky, and N. Dubrovinskaia, Phys. Rev. B **102**, 134109 (2020).

[20] J. Buhot, O. Moulding, T. Muramatsu, I. Osmond, and S. Friedemann, Phys. Rev. B **102**, 104508 (2020).

[21] M. Einaga, M. Sakata, T. Ishikawa, K. Shimizu, M. I. Eremets, A. P. Drozdov, I. A. Troyan, N. Hirao, and Y. Ohishi, Nat. Phys. **12**, 835 (2016).

[22] A. F. Goncharov, S. S. Lobanov, V. B. Prakapenka, and E. Greenberg, Phys. Rev. B **95**, 140101(R) (2017).

[23] S. Villa-Cortés and O. De la Peña-Seaman, J. Phys. Chem. Solids **161**, 110451 (2022).

[24] I. Troyan, A. Gavriliuk, R. Rüffer, A. Chumakov, A. Mironovich, I. Lyubutin, D. Perekalin, A. P. Drozdov, and M. I. Eremets, Science **351**, 1303 (2016).

[25] See Supplemental Material at http://link.aps.org/supplemental/10.1103/PhysRevB.105.L220502 for further details of high-pressure sample synthesis, electrical transport measurements, x-ray diffraction measurements for structural characterization, and DFT calculations.

[26] O. T. Lord, E. T. H. Wann, S. A. Hunt, A. M. Walker, J. Santangeli, M. J. Walter, D. P. Dobson, I. G. Wood, L. Vočadlo, G. Morard, and M. Mezouar, Phys. Earth Planet. Inter. **233**, 13 (2014).

[27] C. Prescher and V. B. Prakapenka, High Press. Res. **35**, 223 (2015).

[28] B. H. Toby and R. B. Von Dreele, J. Appl. Crystallogr. **46**, 544 (2013).

[29] D. Duan, Y. Liu, F. Tian, D. Li, X. Huang, Z. Zhao, H. Yu, B. Liu, W. Tian, and T. Cui, Sci. Rep. **4**, 6968 (2014).

[30] V. V. Struzhkin, R. J. Hemley, H.-K. Mao, and Y. A. Timofeev, Nature (London) **390**, 382 (1997).

[31] E. Gregoryanz, V. V. Struzhkin, R. J. Hemley, M. I. Eremets, H.-k. Mao, and Y. A. Timofeev, Phys. Rev. B **65**, 064504 (2002).

[32] J. M. Ziman, *Electrons and Phonons* (Clarendon Press, Oxford, 1960).

[33] M. Monni, F. Bernardini, A. Sanna, G. Profeta, and S. Massidda, Phys. Rev. B **95**, 064516 (2017).

[34] We find that the ratio B/R_0 is increased by ≈40% for the sulphur contribution after laser heating compared to before laser heating. This suggests that the laser heating has annealed the elemental sulphur and reduced the concentration of dislocations and/or grain boundaries.

[35] M. J. Rice, Phys. Rev. Lett. **20**, 1439 (1968).

[36] P. Blaha, K. Schwarz, G. Madsen, D. Kvasnicka, R. Laskowski, F. Tran, L. Marks, and J. Luitz, *WIEN2k: An Augmented Plane*

Wave Plus Local Orbitals Program for Calculating Crystal Properties (Techn. Universität, Vienna, 2021).

[37] J. P. Perdew, K. Burke, and M. Ernzerhof, Phys. Rev. Lett. **77**, 3865 (1996).

[38] T. Jarlborg and A. Bianconi, Sci. Rep. **6**, 24816 (2016).

[39] J. E. Hirsch and F. Marsiglio, Phys. Rev. B **103**, 134505 (2021).

[40] M. Tinkham, Phys. Rev. Lett. **61**, 1658 (1988).

[41] A. L. Cornelius, K. V. Lawler, and A. Salamat, arXiv:2202.04254 (2022).

[42] M. Eisterer, M. Zehetmayer, and H. W. Weber, Phys. Rev. Lett. **90**, 247002 (2003).

[43] S. Friedemann, Data for "Clean-limit superconductivity in Im3m H3S synthesized from sulphur and hydrogen donor ammonia borane" (2022), doi: 10.5523/bris.31o8e84oir4ug21mx9vqymsjyz.